Supplementary Information (SI) for Energy & Environmental Science.

Supporting Information

Anti-solvent engineering for efficient and stable perovskite solar cells with preferentially orientated 2-dimensional/3-dimensional heterojunctions

Zhinan Zhang[1†], Yinghao Xu[1†], Shaofu Wang[1], Chuan Peng[1], Peiran Liu[1], Shengjie Du[1], Dexin Pu[1], Xingzhong Zhao[1], Minghui Shang[2*], Guojia Fang[1, 3*] and Zhenhua Yu[1*]

[1]School of Physics and Technology, Key Laboratory of Artificial Micro/Nano Structures of Ministry of Education, Wuhan University, Wuhan, 430072 P.R. China

[2]Institute of Micro/Nano Materials and Devices, Ningbo University of Technology, Ningbo, 315211 P.R. China

[3]School of Electronics and Electrical Engineering, Wuhan Textile University, Wuhan, 430020 P.R. China

[†]These authors contributed equally

[*]Correspondence should go to Z. Y. Email: zhyu1989@whu.edu.cn

Experimental Section

Materials: Formamidinium iodide (FAI), 4-Methoxy-phenethylammonium iodide (4-MeO-PEAI), n-Hexylammonium iodide (n-HeXAI) were purchased from greatcell solar. Propane-1, 3-diammonium iodide ($PDAI_2$, ≥98%), lead chloride ($PbCl_2$, 99.999%), cesium iodide (CsI, 99.999%), lead bromide ($PbBr_2$, 99.999%), Dimethyl sulfoxide (DMSO, anhydrous, 99.9%), *N,N*-Dimethylformamide (DMF, anhydrous, 99.8%) were purchased from Sigma-Aldrich. Propylamine hydroiodide (PAI, ≥99.5%), Butylamine hydroiodide (BAI), Methyldiammonium diiodide ($MDAI_2$, 98%), Phenylmethylammonium chloride (PMACl, ≥99.5%), Methylammonium chloride (MACl), Methylammonium bromide (MABr), 2,9-dimethyl-4, 7-diphenyl-1, 10-phenanthroline (BCP), lithium fluoride (LiF) was purchased from Xi'an Yuri Solar. Lead iodide (PbI_2, 99.99%), Dimethoxy-9H -carbazol-9-yl)ethyl]phosphonic acid (MeO-2PACz, 98.0%) were purchased from TCI. Copper (Cu), anhydrous ethanol (AR), and Diethyl ether anhydrous (DE, AR) were purchased from Sinopharm Chemical Reagent. Ultra-dry chlorobenzene (CB), N-(4-carboxyphenyl)guanidine hydrochloride (GuaBCl, 99%), and Ethyl acetate (EA, extra dry, 99.8%) were purchased from Innochem. Anisole (extra dry, 99%) was purchased from Energy Chemical. Isopropanol (IPA, 99.5%) was purchased from Macklin. Fullerene (C60, 99.9%) was purchased from Advanced Election Technology. Toluene (TL, 99.5%) was purchased from Yonghua Chemical. All chemicals were not further purified.

Preparation of the perovskite precursor solution: the 1.5 M perovskite precursor solution was prepared via dissolution of 18.37 mg CsI, 197.86 mg FAI, 6.76 mg MABr, 8.88 mg MACl, 577.15 mg PbI_2, 22.2 mg $PbBr_2$ in 873 μL DMF and DMSO solution (v/v = of 4: 1) and stirring 3 hours at room temperature. Then, 1.1 mg/mL PMACl, 2.1 mg/mL $PbCl_2$, and 1 mg/mL GuaBCl were added into the perovskite precursor solution and stirred for 30 minutes. Finally, the precursor solution was filtered with 0.45 μm poly(tetrafluoroethylene) (PTFE) filters.

Device Fabrication: The indium tin oxide (ITO) glass substrates were washed in IPA and acetone by ultrasonic treatment for 20 min, respectively. Then, the ITO substrates were treated with UV-ozone (UVO) for 15 min. The ethanol solution of MeO-2PACz was spin-coated onto the ITO glass substrates at 5000 rpm for 20 s, followed by annealing at 110 °C for 10 min to fabricate the self-assembled monolayer (SAM). The perovskite precursor solution was spin-coated on SAM at 1000 rpm for 10 s, then, 200 μL CB or TL: DE@IPA = 4: 1@10% or n-HeXAI and 4-MeO-PEAI in TL: DE@IPA (n-HeXAI: 4-MeO-PEAI = 9: 1, 1.5 mg/mL in IPA) were rapidly added to the top of the perovskite at 3000 rpm for 30 s, 15 s before the end of the spin-coating process. The film was annealed at 110 °C for 15 min. For surface passivation, The IPA solution of $PDAI_2$ was cast onto 5000 rpm spun perovskite films, followed by annealing at 110 °C for 10 min. Finally, 2.5 nm LiF, 18 nm C60, 4.5 nm BCP, and 80 nm copper electrodes were sequentially thermal evaporated onto these perovskite films.

Perovskite mini-module fabrication: The perovskite solar modules (PSMs) consisting of 6 sub-cells connected in series were fabricated on ITO glass substrates with dimensions of 6.0 cm × 6.0 cm. The series interconnection of the mini-module was accomplished by means of P1, P2, and P3 lines, which were scribed with a laser scribing system of 1064 nm at a power of 20 W. The P1 lines (a width of 27 μm) were pre-patterned on the ITO glass substrates by utilizing 28% of a laser power under a speed of 400 mm/s with a frequency of 100 kHz and a pulse duration of 120 ns. The ITO substrate was cleaned with organic solvent and treated with UVO for 15 min. Compared to the fabrication of hole transport layer (HTL), perovskite and surface passivation layers for small area solar cells, except for a corresponding increase in the amount of solution, other parameters remain unchanged. Subsequently, 30 nm C60 and 30 nm SnO_2 were sequentially thermal evaporated and atomic layer deposition onto these perovskite films. Before the copper electrode deposition process step, the P2 lines (a width of 50 μm) were patterned. This was accomplished at an average laser power of 29% under a speed of 400 mm/s with a frequency of 500 kHz and a pulse duration of 120 ns. When the 100 nm thick copper electrode was deposited, the P3 lines (a width of 45 μm) were patterned following the same scribing conditions as the P2 lines.

Electrical Measurements: Current density and voltage curves (*J*-*V*) were performed by utilizing a Keithley 2450 primary meter, and the light source was the simulated AM1.5G irradiation (100 mW/cm^2) generated via the xenon-lamp-based ZOliX SS150 solar simulator. The light intensity was calibrated by a standard silicon solar cell. All *J*-*V* curves were obtained in reverse scan mode with a scan rate of 0.04 V/s. The EQE measurements were carried out with the Enli QE measurement kit (Enli Technology Co., Ltd) and samples were calibrated by standard reference silicon solar cells with a known EQE. Unless specified, all perovskite solar cells had an operating area of 9 mm^2, which was determined by the overlap area of the ITO and Cu electrodes. All devices were encapsulated by utilizing exopy and cover glass in nitrogen-filled glove box. All measurements of the encapsulated devices were performed in the air environment.

Stability testing: The illumination source is white light-emitting diode (LED) with its intensity calibrated to match 1-sun conditions. For the ISOS-D-1 ageing test, the encapsulated cells were placed at dark storage and open-circuit voltage with temperature of 15-35 °C. To perform operational stability tests of the encapsulated devices, we kept the devices at 55-65 °C in the nitrogen gas. The encapsulated devices were measured periodically after 20 min cooling in ambient air. The operational stability of the encapsulated PSCs was measured by a home-made stability test system operating in the MPP tracking mode. The device performance was evaluated periodically.

Characterization: The scanning electron microscope (SEM) images were taken by using ZEISS GeminiSEM 500. The X-ray diffraction pattern (XRD) was taken from Rigaku Smartlab with X-ray generator at 3 KW assisted by copper Kα radiation (λ = 1.5418 Å) with the scanning range and scanning speeds are 5° to 50° and 5 degrees/min. The UV-vis-NIR absorbance spectrum was performed by using PerkinElmer Lambda 650S UV-vis-NIR Spectrophotometers. The photoluminescence (PL) spectrum and time-resolved photoluminescence (TRPL) spectrum were carried out on the HORIBA Delta Flex fluorescence spectrometer. A 372 nm laser was utilized as an excitation source to collect signals at 700-900 nm. Atomic force microscope (AFM) and kelvin probe force microscopy (KPFM) images were performed by Bruker Dimension Icon XR equipment in Scanasyst-Air and Peak force KPFM mode. X-ray photoelectron spectroscopy (XPS) was characterized by Thermo Fisher Scientific K-Alpha and XPS spectra were calibrated by the reference C *1s* level at 284.8 eV. Ultraviolet photoelectron spectroscopy (UPS) was conducted in Thermo Fisher Scientific K-Alpha system with a He Iα photon source (h_v = 21.22 eV) and a bias voltage of -5 V. All of the UPS and XPS spectra were processed and fitted via Advantage software. Light intensity-dependent measurements for ideality factors were measured with a series of neutral optical density filters. The Mott-Schottky analysis and Electrochemical impedance spectroscopy (EIS) were measured by the CHI 660E potentiostat system.

Time-of-Flight Secondary Ion Mass Spectrometry (TOF-SIMS): Depth profiling of perovskite films was carried out by utilizing an ION-TOF TOF-SIMS V time-of-flight SIMS (TOF-SIMS) spectrometer. Analysis was completed by utilizing a 30 kV Bi primary ion gun. High mass resolution depth profiles were completed with a 30 KeV Bi^{3+} primary ion beam (1.0 pA pulsed beam current) and the analysis area was 100 × 100 μm. The primary ion beam dose density was kept below 7.2×10^{13} ions/cm^2 to remain under the static-sims limit. Sputter depth profiling was accomplished with a 1 keV O_2 ion beam (110 nA sputter current) and the sputter area was 300 × 300 μm.

Grazing-incidence wide-angle X-ray scattering (GIWAXS): The GIWAXS patterns were obtained by Xenocs Xeuss 2.0 under the incidence angle of 2°. The X-ray generator power was 30 W and was assisted by copper radiation (λ = 1.54189 Å). The pixel size was 172 × 172 μm and the distance between the detector and sample was 150 mm. The data were recorded by utilizing the detector of Pilatus 3R 300K.

Computing Methods: Geometrical optimization and electronic configuration calculations were performed using the Vienna ab initio simulation package (VASP)[1] within the framework of density functional theory.[2, 3] Standard Perdew-Burke-Ernzerhof (PBE) functionals[4] were utilized for energy minimization. The interactions between valence electrons and ion cores were treated with ultrasoft pseudopotentials. The Pb $5d^{10}6s^{2}6p^{2}$, I $5s^{2}5p^{5}$, N $2s^{2}2p^{3}$, C $2s^{2}2p^{2}$ and H $1s^{1}$ atomic orbitals were treated as valence orbitals[5]. The valence electron wave functions were expanded in plane-wave basis sets with a cutoff energy of 450 eV. A 2 × 2 × 1 Monkhorst-Pack k-point mesh was applied for sampling the first Brillouin zone of the supercell with the dimension of 12.65 × 12.72 × 41.10 (Å^{3}). The vacuum thickness was set to 15 Å for slab model sampling the surface, which is enough to avoid the interaction between image layers. The energy minimization stopping criterion was less than 1.0×10^{-5} eV per atom. The atomic positions were fully relaxed until the residual forces below 0.03 eV Å^{-1}. And the electronic structures were self-consistently calculated based on the relaxed configures. The charge density difference was computed with aid of the vaspkit developed by V. Wang et. al.[5]

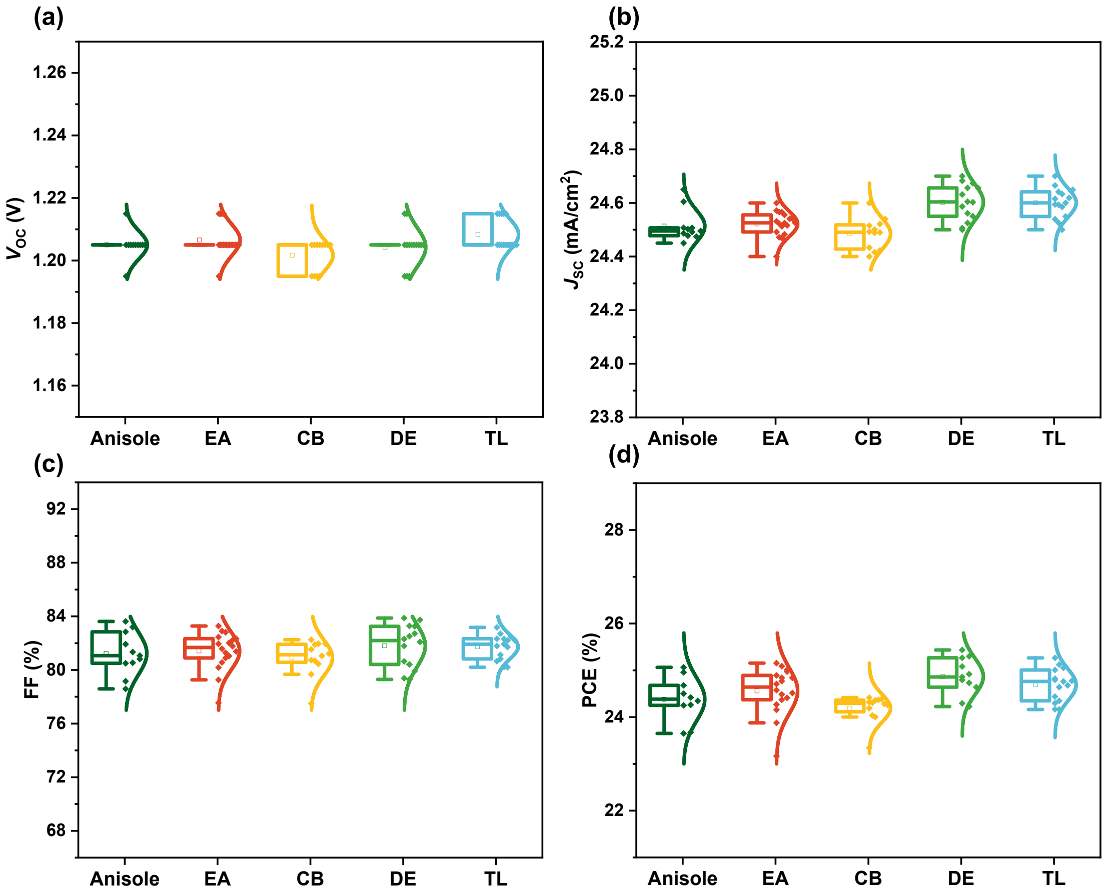

Figure S1. The statistics of photovoltaic parameters derived from the *J-V* characteristic curves of devices based on different anti-solvents (anisole, EA, CB, DE, TL). For each type of anti-solvent, five devices were fabricated to analyze the photovoltaic parameters. The photovoltaic parameters of all the PSCs were determined by *J-V* measurements at a scan condition of 0.04 V/s.

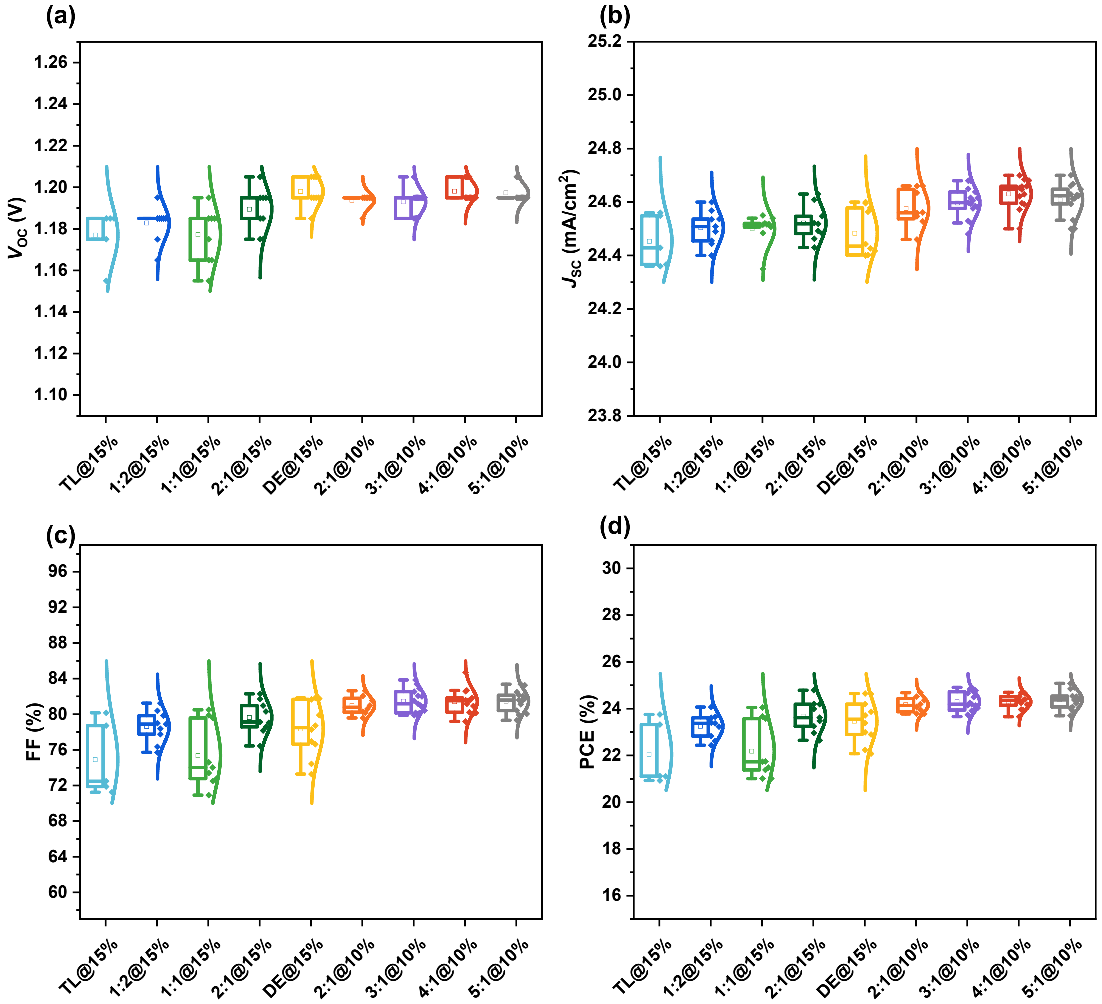

Figure S2. The statistics of photovoltaic parameters derived from the *J*-*V* characteristic curves of devices based on the varied ratio of the hybrid anti-solvent. The specific meaning of the horizontal coordinate is the volume ratio of anti-solvent DE, TL and IPA: DE: TL@IPA.

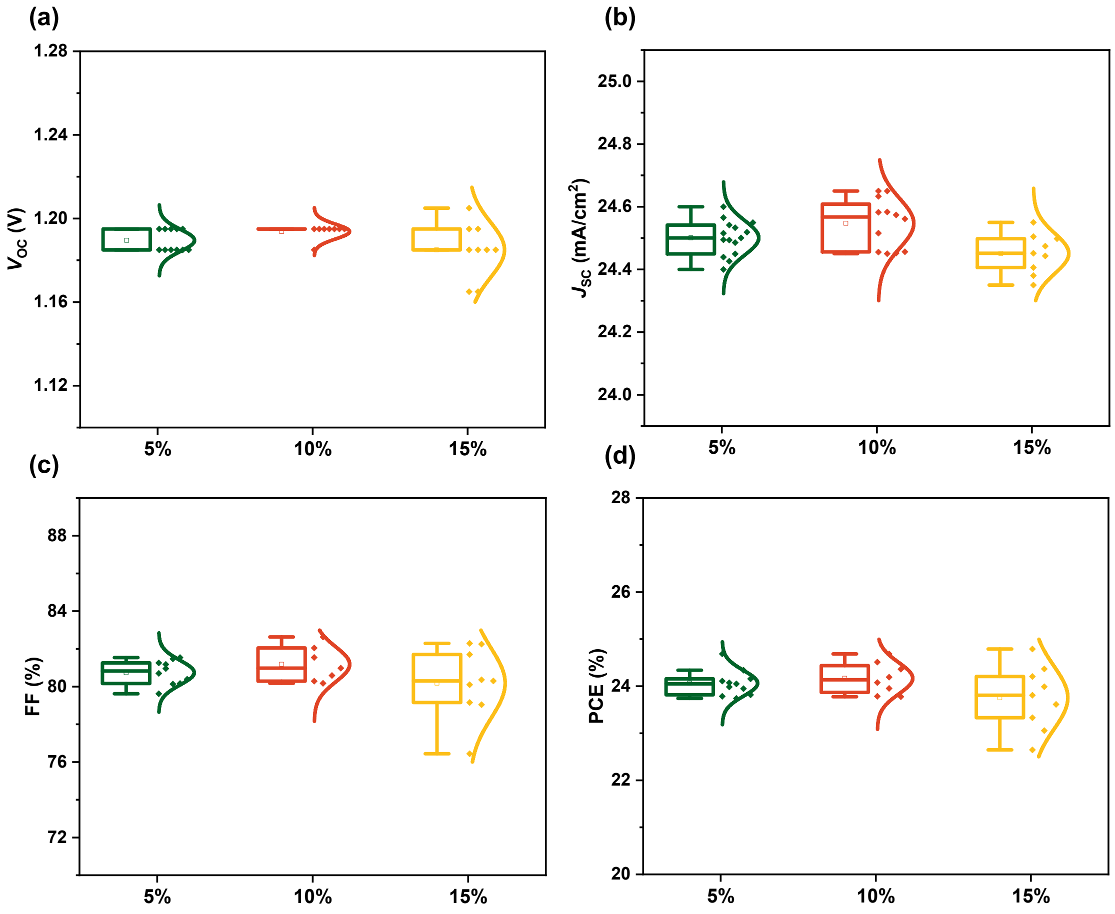

Figure S3. The statistics of photovoltaic parameters derived from the *J-V* characteristic curves of devices with different IPA volume ratios in the hybrid anti-solvent. The volume ratio of anti-solvent DE: TL is 2: 1.

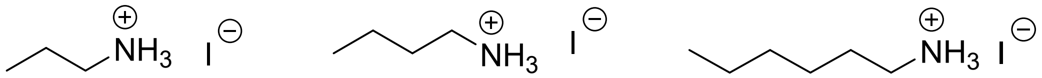

PAI **BAI** **n-HeXAI**

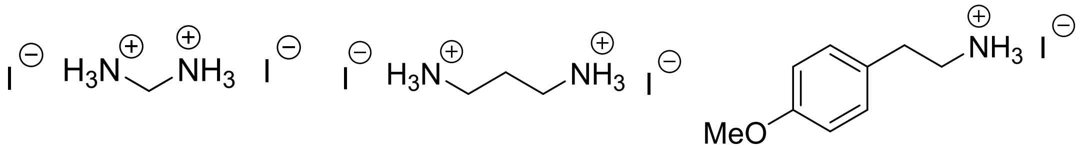

MDAI$_2$ **PDAI$_2$** **4-MeO-PEAI**

Figure S4. The chemical structures of the ammonium ligands.

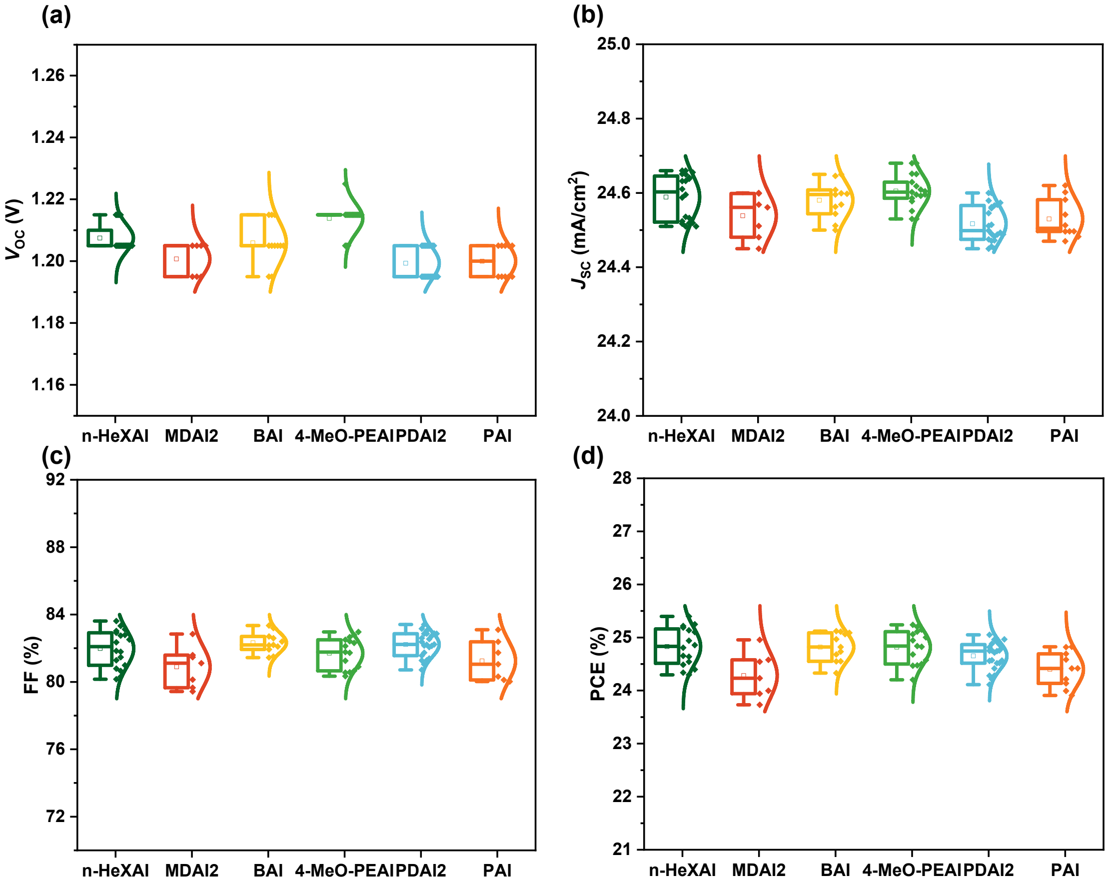

Figure S5. The statistics of photovoltaic parameters derived from the *J*-*V* characteristic curves of devices based on different 2D materials in the hybrid anti-solvent (volume ratio of DE: TL@IPA = 4:1@10%).

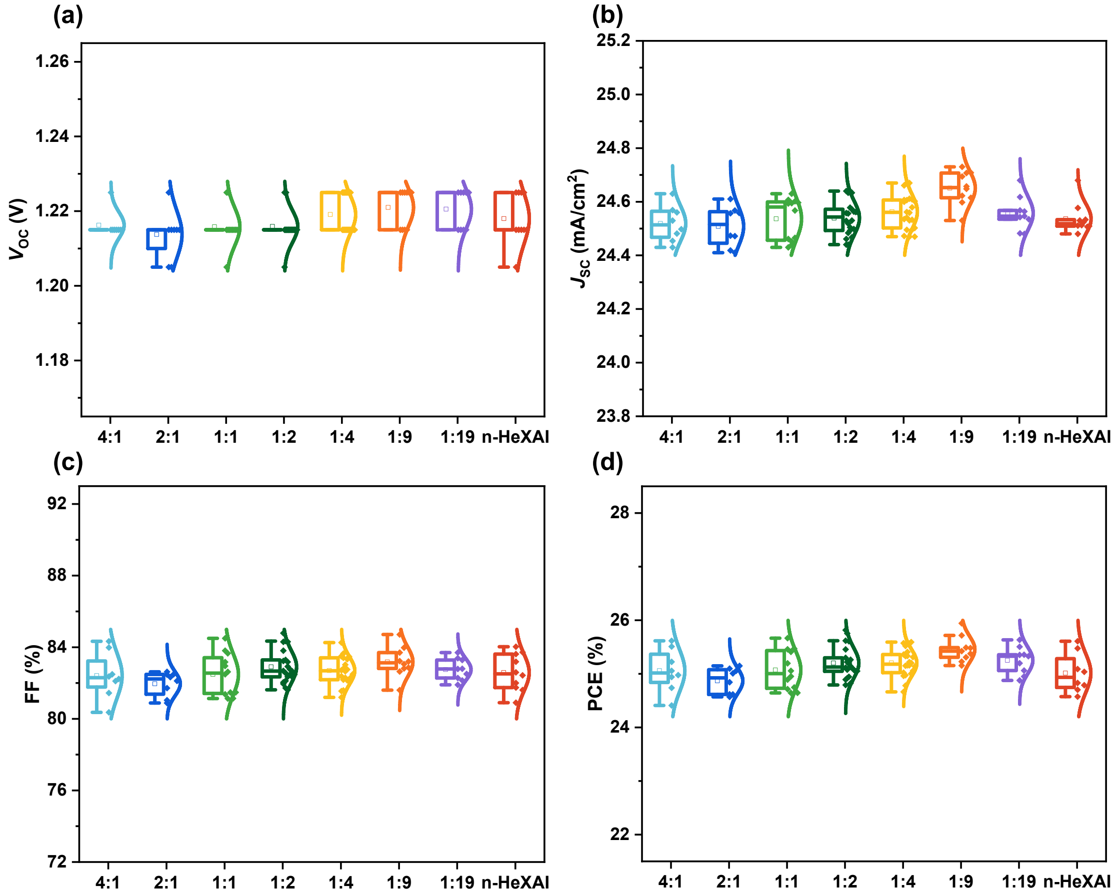

Figure S6. The statistics of photovoltaic parameters derived from the *J-V* characteristic curves of devices based on the varied ratio of 2D materials in the hybrid anti-solvent (volume ratio of DE: TL@IPA = 4:1@10%). The specific meaning of the horizontal coordinate is the volume ratio of 4-MeO-PEAI and n-HeXAI.

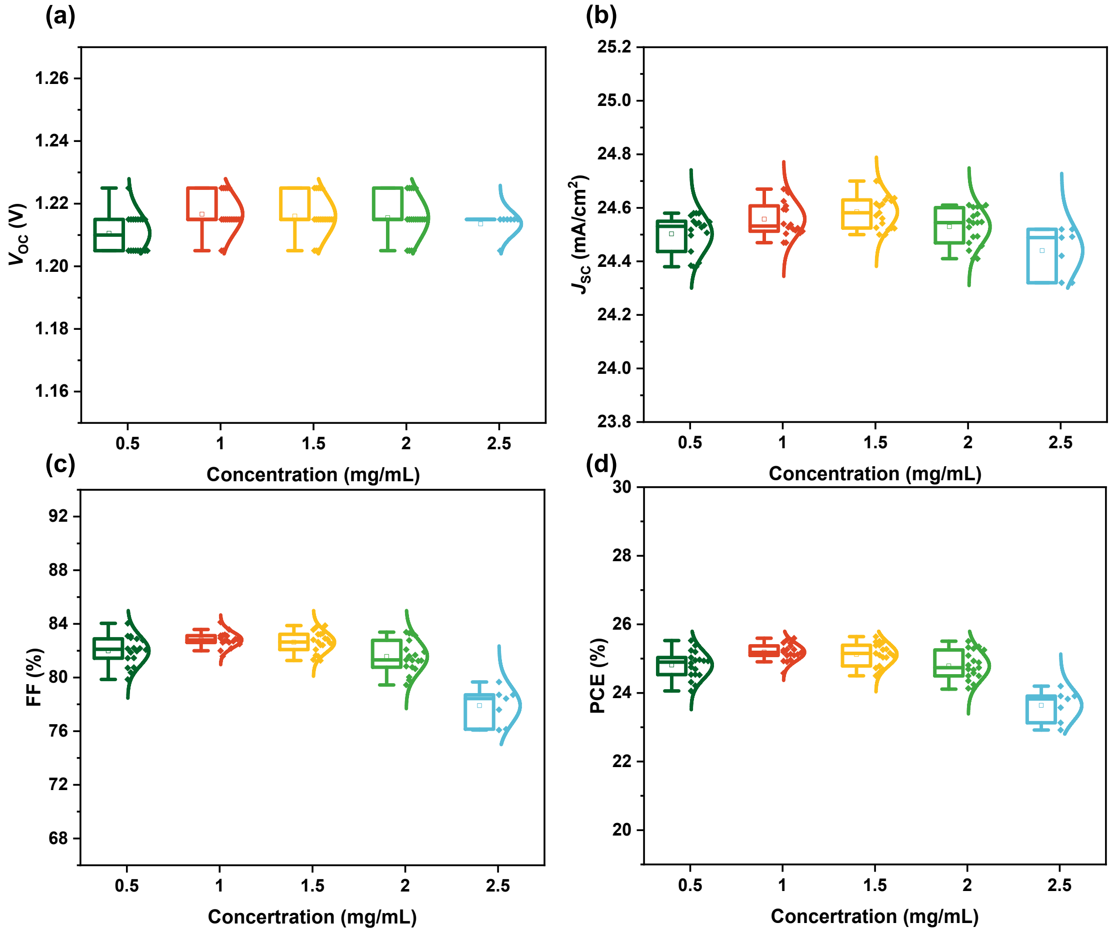

Figure S7. The statistics of photovoltaic parameters derived from the *J-V* characteristic curves of devices based on different concentrations of the mixed 2D materials (4-MeO-PEAI: n-HeXAI = 1: 9) in the hybrid anti-solvent (DE: TL@IPA = 4:1@10%).

福建省计量科学研究院
FUJIAN METROLOGY INSTITUTE
（国家光伏产业计量测试中心）
National PV Industry Measurement and Testing Center

中国认可 国际互认 检测 TESTING CNAS L0131

检 测 报 告
Test Report

报告编号：24Q3-00468
Report No.

客户信息 Name of Custome	武汉大学/无锡永珈光能科技有限公司
联络信息 Contact Information	武汉大学物理学院老楼C314&江阴市青阳镇青桐路215号霞客湾创智园3幢3层
物品名称 Name of items	单结钙钛矿电池（IV）
型号/规格 Type /Specification	1.5 cm x 1.5 cm
物品编号 Items No	2#
制造厂商 Manufacturer	武汉大学/无锡永珈光能科技有限公司
物品接收日期 Items Receipt Date	2024-07-29
检测日期 Test Date	2024-07-31

福建省计量科学研究院 证书/报告专用章 Stamp 3501020056403

批准人： Approved by	黎健生	黎健生
核验员： Checked by	何翔	何翔
检测员： Test by	陈彩云	陈彩云

发布日期：2024 年 08 月 05 日
Date of Report Year Month Day

扫一扫 查真伪

本院/本中心地址：福州市屏东路9-3号
Address：9-3 Pingdong Road,Fuzhou,China
电话：0591-87845050
Telephone
传真：0591-87808417
Fax
邮编：350003
Post Code
网址：www.fjjl.net
Web Site
咨询电话：0591-87845050
Inquire line
投诉电话：0591-87823025
Complaint Tel

未经本院/本中心书面批准，部分采用本报告内容无效。
Partly using this Report will not be admitted unless allowed by FMI/ Center.

第 1 页/共 6 页
Page of Pages

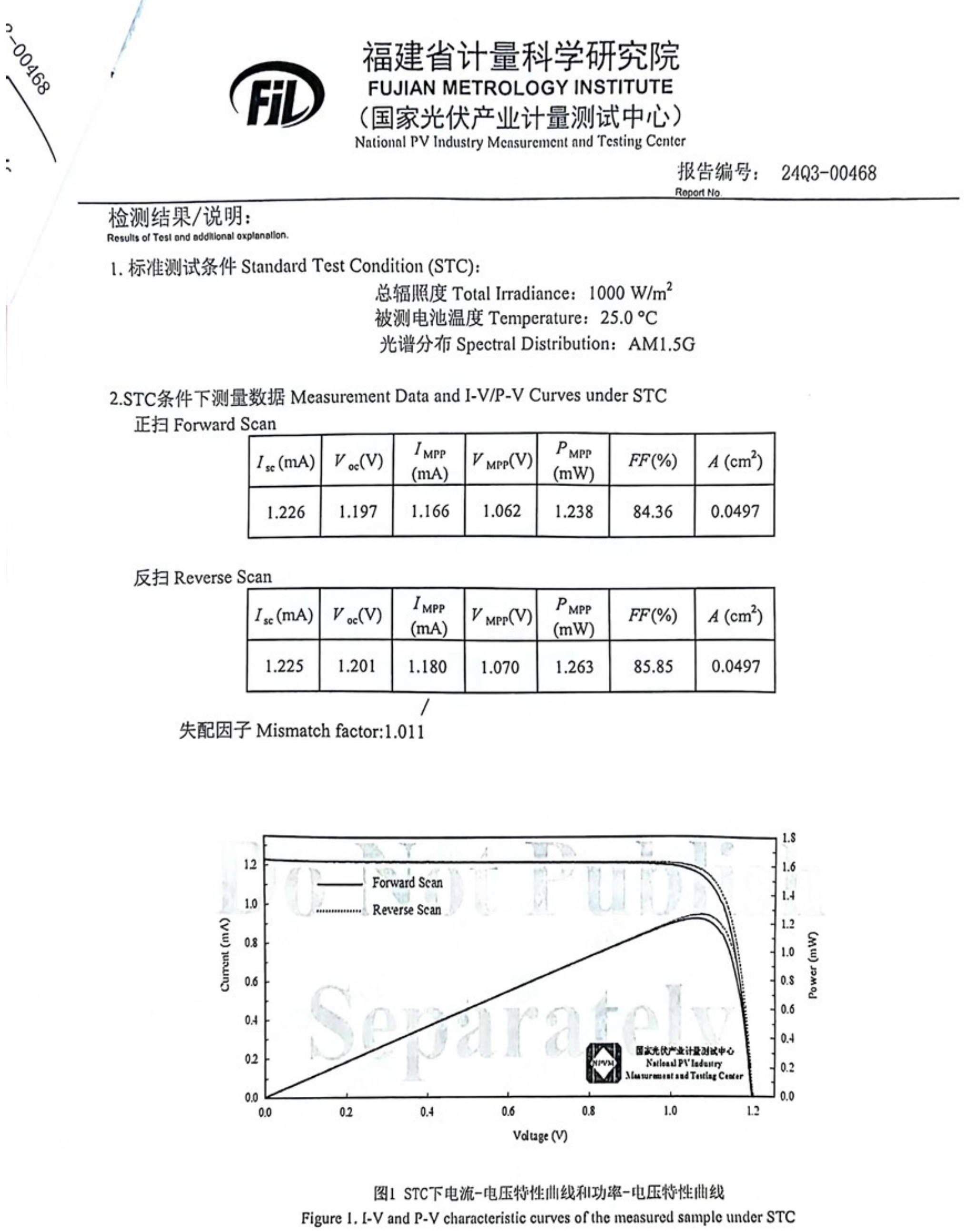

福建省计量科学研究院
FUJIAN METROLOGY INSTITUTE
（国家光伏产业计量测试中心）
National PV Industry Measurement and Testing Center

报告编号： 24Q3-00468
Report No.

检测结果/说明：
Results of Test and additional explanation.

1. 标准测试条件 Standard Test Condition (STC):

总辐照度 Total Irradiance：1000 W/m^2
被测电池温度 Temperature：25.0 °C
光谱分布 Spectral Distribution：AM1.5G

2.STC条件下测量数据 Measurement Data and I-V/P-V Curves under STC

正扫 Forward Scan

I_{sc} (mA)	V_{oc}(V)	I_{MPP} (mA)	V_{MPP}(V)	P_{MPP} (mW)	FF(%)	A (cm^2)
1.226	1.197	1.166	1.062	1.238	84.36	0.0497

反扫 Reverse Scan

I_{sc} (mA)	V_{oc}(V)	I_{MPP} (mA)	V_{MPP}(V)	P_{MPP} (mW)	FF(%)	A (cm^2)
1.225	1.201	1.180	1.070	1.263	85.85	0.0497

失配因子 Mismatch factor:1.011

图1 STC下电流-电压特性曲线和功率-电压特性曲线
Figure 1. I-V and P-V characteristic curves of the measured sample under STC

检测报告续页专用
Continued page of test report

第 3 页/共 6 页
Page of Pages

Figure S8. The certified results of the champion device were measured at the National PV Industry Measurement and Testing Center. The certified PCE is 25.42% certified aperture with an area of 0.0497 cm^2. The certified J-V curves with double scanning give PCE forward: 24.91% and PCE reverse: 25.42%.

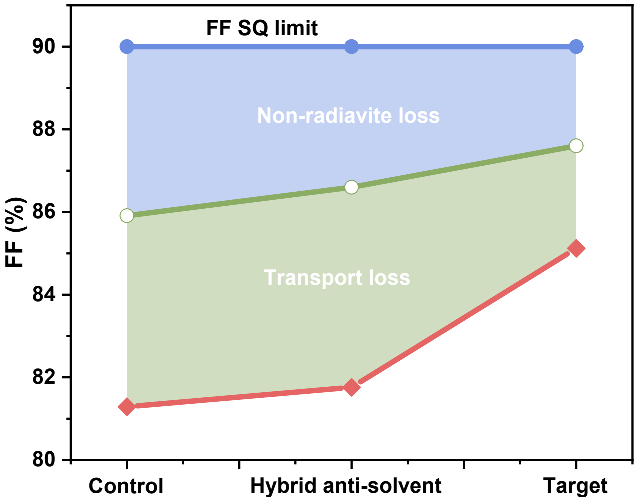

Figure S9. The FF loss analysis for control, hybrid anti-solvent and 4-MeO-PEAI and n-HeXAI modified PSCs.

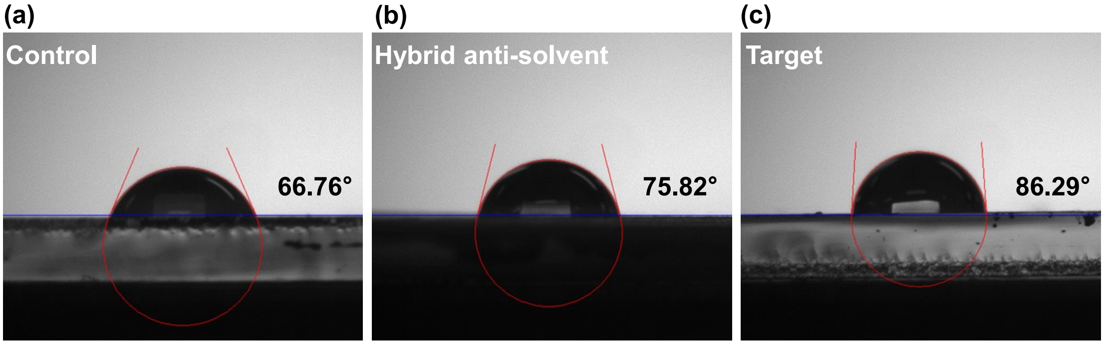

Figure S10. Water contact angles of the control, hybrid anti-solvent and 4-MeO-PEAI and n-HeXAI modified perovskite films.

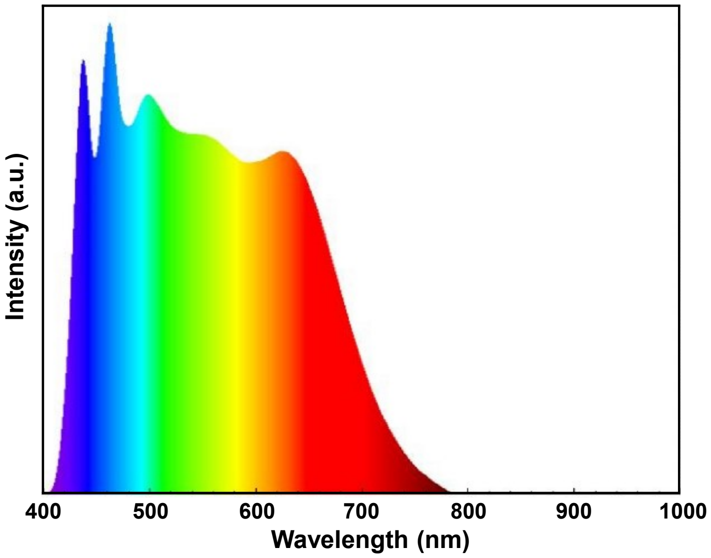

Figure S11. The spectrum of white light-emitting diode (LED) for stability testing.

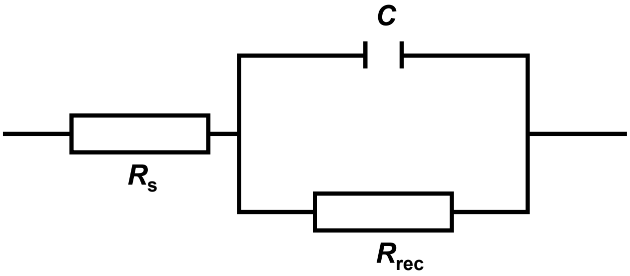

Figure S12. The equivalent circuit model for electrochemical impedance spectroscopy (EIS) fitting of PSC, which includes series resistance (R_s), recombination resistance (R_{rec}) and capacitance (C).

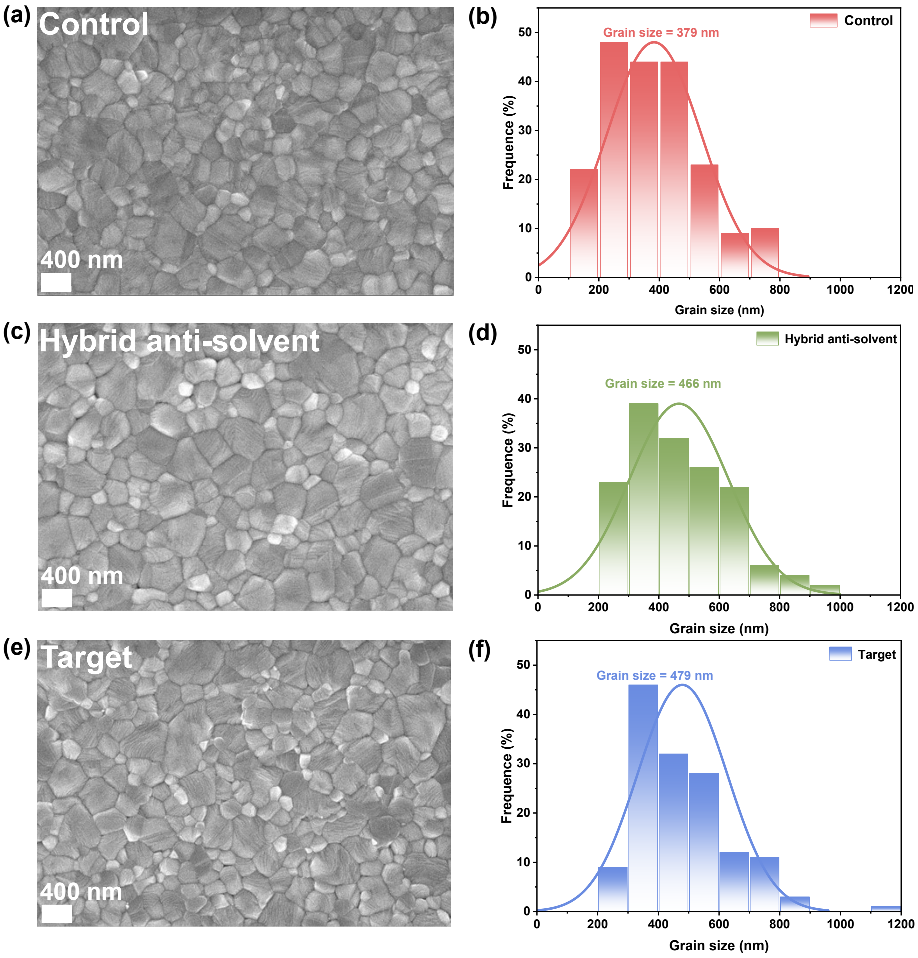

Figure S13. SEM images of (a) control, (c) hybrid anti-solvent and (e) 4-MeO-PEAI and n-HeXAI modified perovskite films. Grain size analysis of (b) control, (d) hybrid anti-solvent and (f) 4-MeO-PEAI and n-HeXAI modified perovskite films.

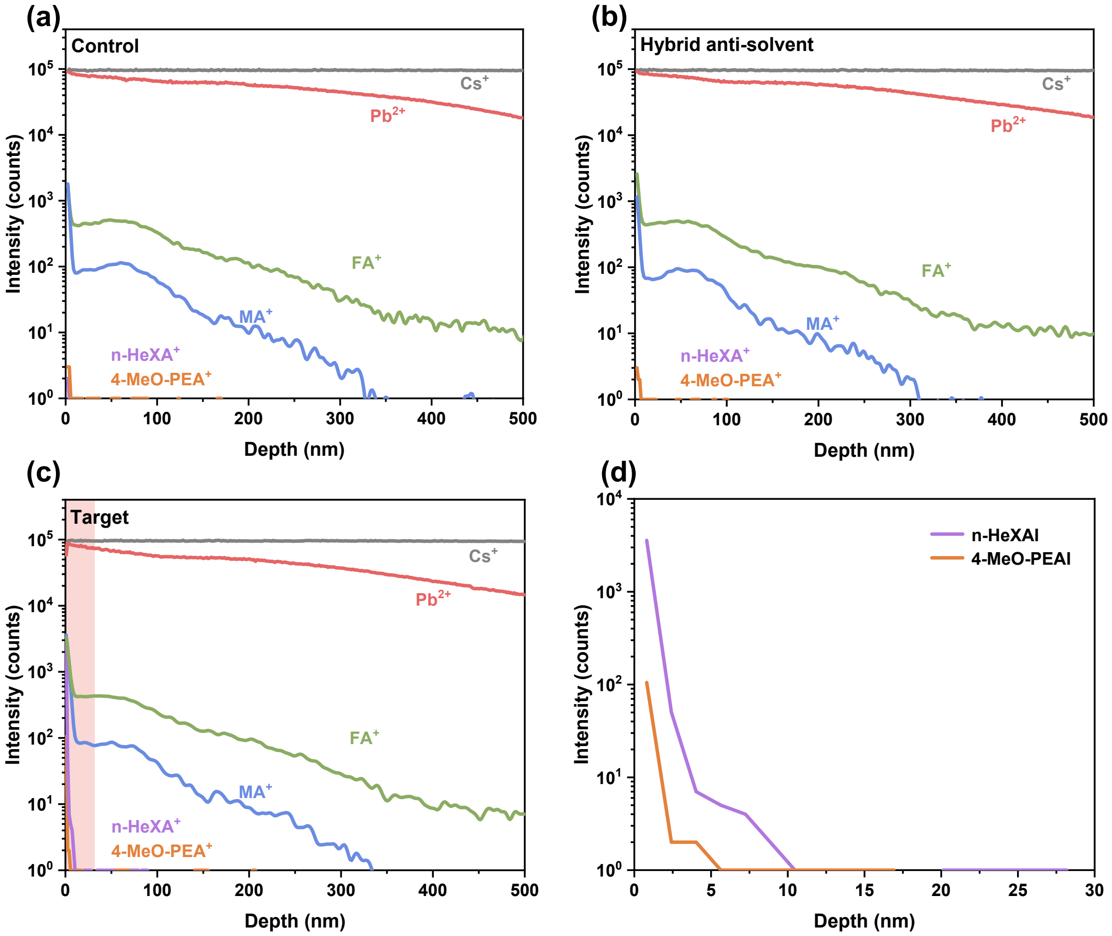

Figure S14. TOF-SIMS profile of the (a) control, (b) hybrid anti-solvent and (c) 4-MeO-PEAI and n-HeXAI modified perovskite films from the glass/ITO/MeO-2PACz/perovskite. (d) The depth profiles of 4-MeO-PEA$^+$ and n-HeXA$^+$ ions were obtained from TOF-SIMS.

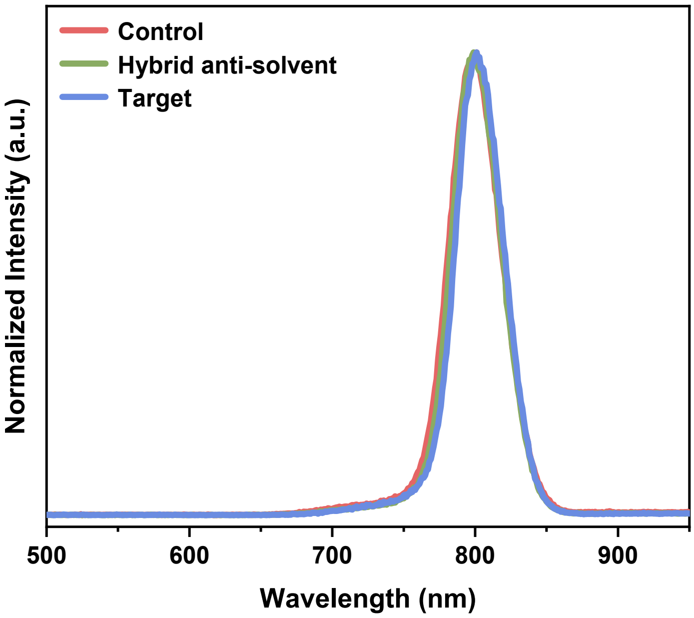

Figure S15. The normalized PL spectra of the control, hybrid anti-solvent and 4-MeO-PEAI and n-HeXAI modified perovskite films ranged from 500 nm to 950 nm.

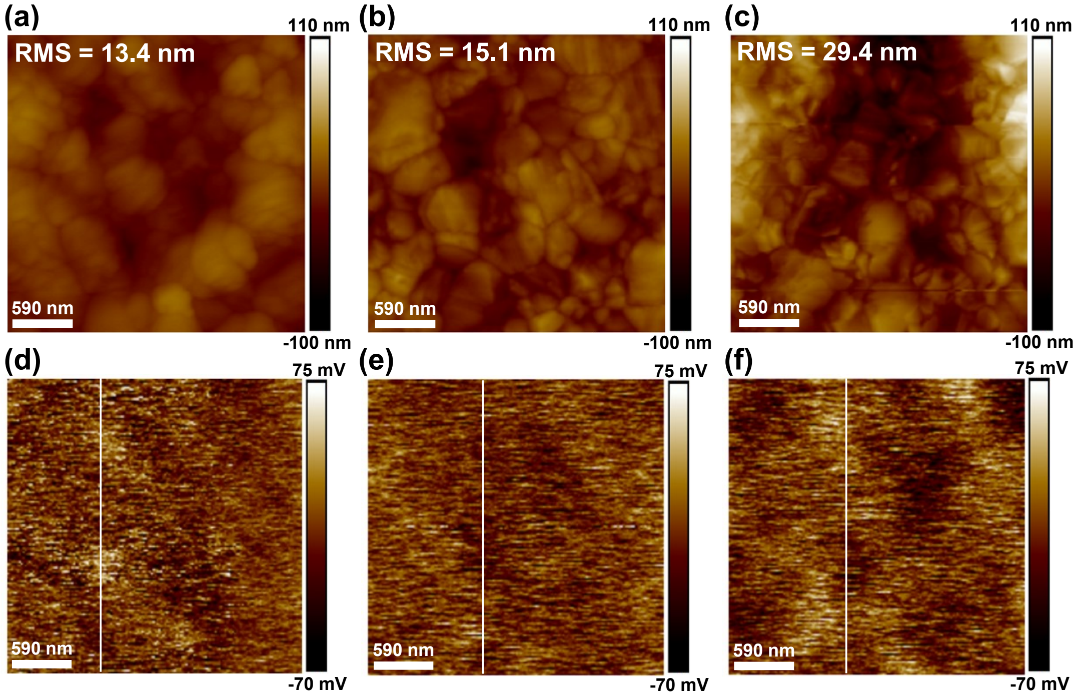

Figure S16. (a, b, c) The AFM images and (d, e, f) two-dimensional surface potential images were measured by utilizing KPFM for control, hybrid anti-solvent and 4-MeO-PEAI and n-HeXAI modified perovskite films with 4 μm × 4 μm area size.

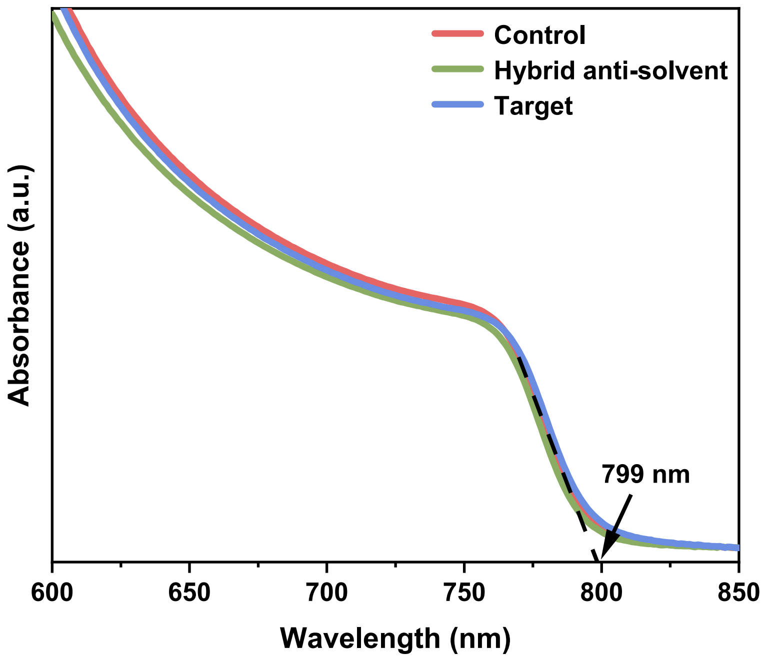

Figure S17. UV-vis spectra of the control, hybrid anti-solvent and 4-MeO-PEAI and n-HeXAI modified perovskite films.

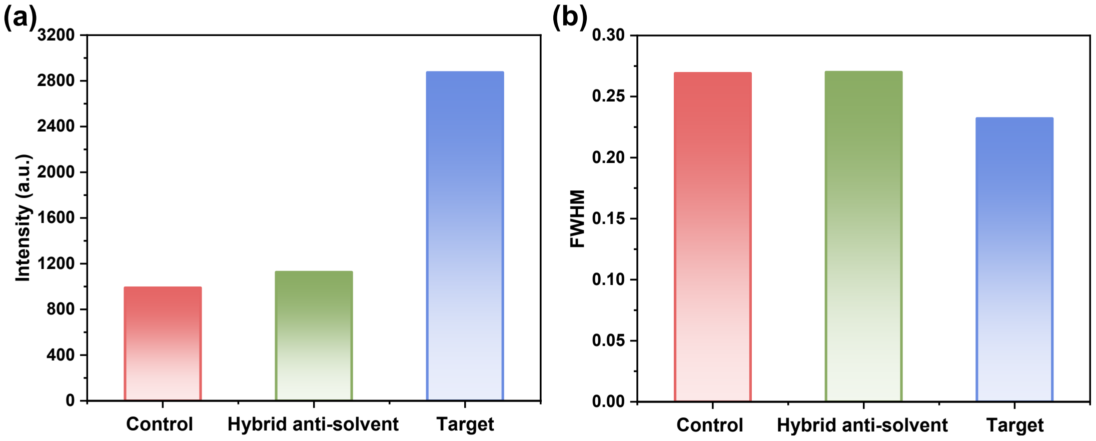

Figure S18. (a) The intensity of (001) diffraction peaks and (b) corresponding full width of half-maximum (FWHM) obtained from XRD spectra for control, hybrid anti-solvent and 4-MeO-PEAI and n-HeXAI modified perovskite films.

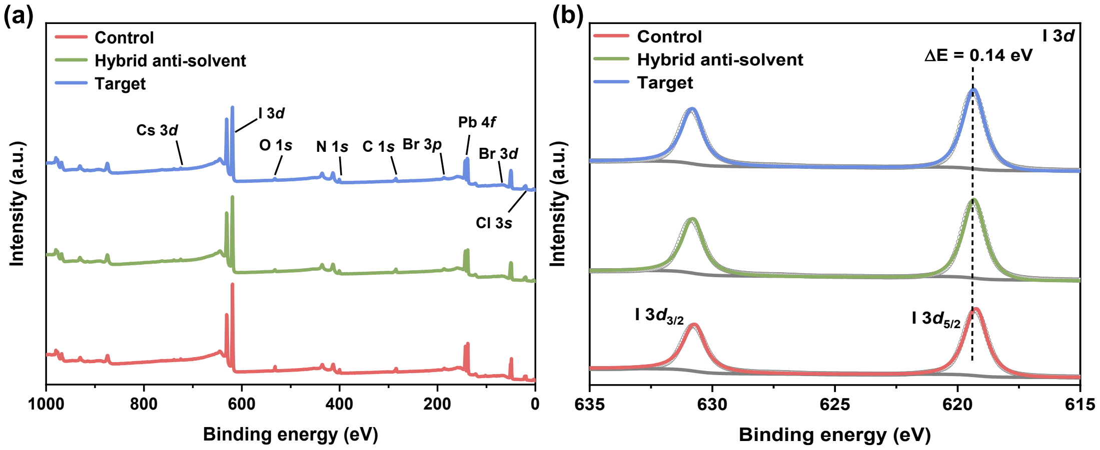

Figure S19. (a) The XPS survey spectra and (b) XPS spectra of I 3*d* the control, hybrid anti-solvent and 4-MeO-PEAI and n-HeXAI modified perovskite films.

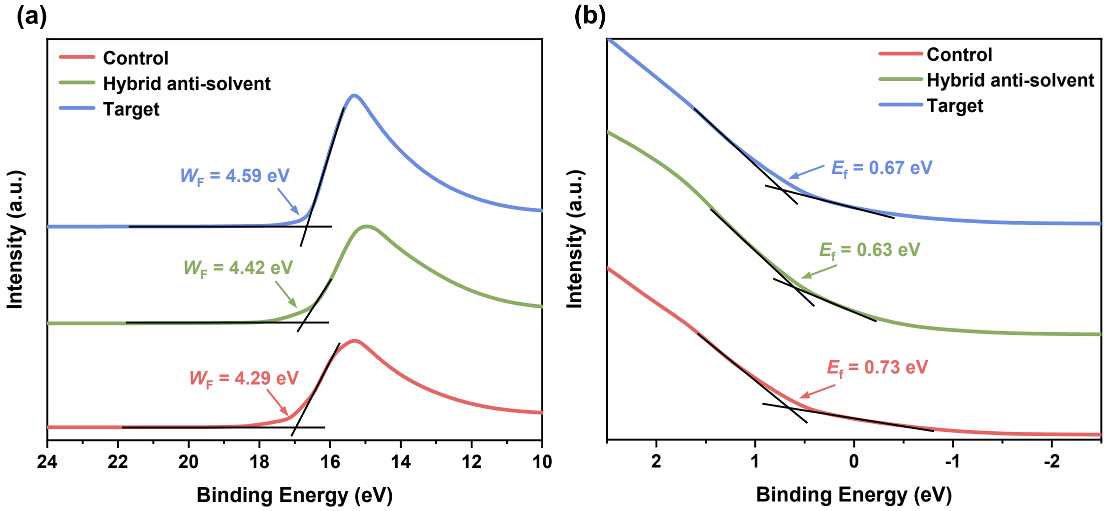

Figure S20. (a) UPS spectra of the cut-off region and (b) UPS spectra of onset region for the control, hybrid anti-solvent and 4-MeO-PEAI and n-HeXAI modified perovskite films.

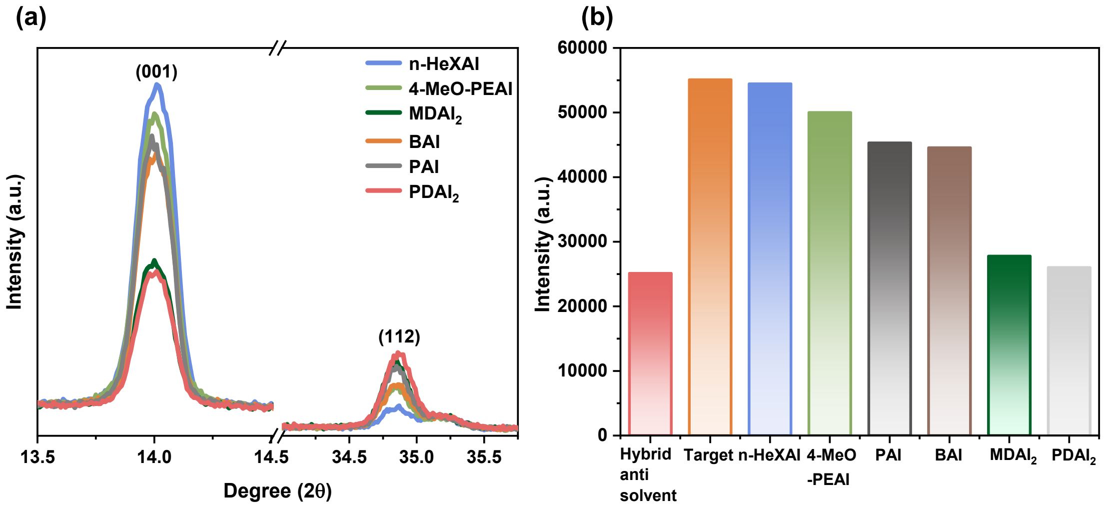

Figure S21. (a) The XRD spectra of (001) and (112) crystalline surfaces and (b) the intensity of (001) diffraction peaks for hybrid anti-solvent, 4-MeO-PEAI modified, n-HeXAI modified, 4-MeO-PEAI and n-HeXAI modified, PAI modified, BAI modified, $PDAI_2$ modified, $MDAI_2$ modified perovskite films.

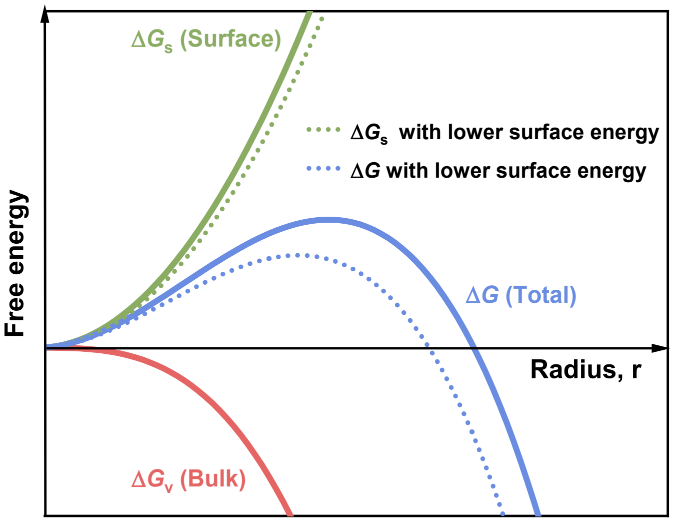

Figure S22. Schematic of free energy as a function of particle radius in classical nucleation theory.

Table S1. Summary of certified inverted (p-i-n) and regular (n-i-p) perovskite solar cells in last one year. *N (%) represents the V_{oc} × FF relative to the S-Q limits of its corresponding band gap.

Structure	E_g (eV)	V_{OC} (V)	FF (%)	V_{OC} × FF	*N (%)	Organ-ization	Type	Ref.
n-i-p	1.54	1.174	84.23	98.84	87.55	NIM	Fast-scan	6
n-i-p	1.54	1.1799	83.10	98.05	86.85	Newport	Fast-scan	7
n-i-p	1.55	1.178	85.45	100.66	88.43	SIMIT	Fast-scan	8
n-i-p	1.52	1.1835	84.04	99.46	89.56	DGTP	Fast-scan	9
n-i-p	1.55	1.197	82.67	98.96	86.94	NPVM	Fast-scan	10
n-i-p	1.52	1.178	83.6	98.48	88.67	NPVM	Fast-scan	11
n-i-p	1.54	1.191	84.2	100.28	88.82	JET	Fast-scan	12
n-i-p	1.54	1.185	84.2	99.78	88.38	NPVM	Fast-scan	13
n-i-p	1.55	1.147	84.9	97.38	85.55	SIMIT	Fast-scan	14
n-i-p	1.52	1.186	84.98	100.79	90.75	NPVM	Fast-scan	15
n-i-p	/	1.170	82.63	96.68	/	NIM	Fast-scan	16
p-i-n	1.53	1.179	84.13	99.19	88.56	SIMIT	Fast-scan	17
p-i-n	1.55	1.155	85.68	98.96	86.94	NPVM	Fast-scan	18
p-i-n	1.54	1.197	83.33	99.75	88.35	PWQC	Fast-scan	19
p-i-n	1.55	1.179	83.32	98.23	86.30	SIMIT	Fast-scan	20
p-i-n	1.53	1.17	83.14	97.27	86.85	SIMIT	Fast-scan	21
p-i-n	1.55	1.17	84.95	99.39	87.31	SIMIT	Fast-scan	22
p-i-n	1.53	1.167	85.72	100.04	89.32	Enli Tech	Fast-scan	23
p-i-n	/	1.187	82.37	97.77	/	NIM	Fast-scan	24
p-i-n	/	1.188	84.17	99.99	/	SIMIT	Fast-scan	25
p-i-n	1.53	1.192	84.11	100.26	89.52	NPVM	Fast-scan	26
p-i-n	1.54	1.165	84.45	98.38	87.14	PWQC	Fast-scan	27
p-i-n	1.56	1.21	84.65	102.43	89.25	SIMIT	Fast-scan	28

p-i-n	1.56	1.1595	83.05	96.3	83.9	NREL	QSS	29
p-i-n	1.55	1.176	84.91	99.85	87.72	SIMIT	Fast-scan	30
p-i-n	1.52	1.1834	81.2	96.09	86.52	Newport	QSS	31
p-i-n	1.55	1.158	84.01	97.28	85.46	SIMIT	Fast-scan	32
p-i-n	1.50	1.1698	83.47	97.64	89.39	NREL	QSS	33
p-i-n	1.53	1.174	85.2	100.03	89.31	Newport	QSS	34
p-i-n	1.53	1.19	83.61	99.5	88.84	SIMIT	Fast-scan	35
p-i-n	**1.55**	**1.201**	**85.85**	**103.11**	**90.6**	**NPVM**	**Fast-scan**	**This work**

Table S2. Summary of mini-module efficiency from the top journal in the last one year.

Structure	Active area (cm^2)	V_{OC} (V)	I_{SC} (mA)	FF (%)	PCE (%)	Ref.
n-i-p	27.60	——	——	——	22.90	36
p-i-n	7.20	6.82	29.20	77.40	21.40	27
p-i-n	14.65	6.90	56.70	78.70	21.00	31
n-i-p	14.00	——	——	——	17.64	37
n-i-p	18.00	8.91	54.9	76.4	20.76	38
n-i-p	14.40	4.39	92.30	76.31	21.45	39
n-i-p	15.64	9.02	49.89	76.52	22.00	40
n-i-p	10.28	5.88	48.93	75.96	20.66	41
n-i-p	25.00	11.89	59.00	80.22	22.47	42
p-i-n	12.60	5.37	55.57	63.39	15.01	43
n-i-p	25.00	7.91	85.00	67.50	18.16	44
n-i-p	16.80	6.98	67.20	80.03	22.34	45
n-i-p	10.40	6.61	43.89	75.35	21.02	46
p-i-n	**12.40**	**7.09**	**50.64**	**78.00**	**22.59**	**This work**

Table S3. The fitting results of TRPL curves for control, hybrid anti-solvent, 4-MeO-PEAI and n-HeXAI modified perovskite films.

Samples	A_1	τ_1 (ns)	A_2	τ_2 (ns)	τ_{ave} (ns)
Control	11906	11	1525	116	71.5
Hybrid anti-solvent	10537	13	1291	152	94.4
Target	13346	11.75	895	179	96.2

Table S4. The fitting recombination resistance (R_{rec}) of the device in the Nyquist plot.

Samples	R_{rec} (Ω)
Control	79.92
Hybrid anti-solvent	363.16
Target	626.96

Table S5. Calculated valence band (E_{VB}), conduction band (E_{CB}) and $E_{F\text{-edge}}$ from $E_{cut\text{-}off}$, E_{onset} and E_g for the control, hybrid anti-solvent, 4-MeO-PEAI and n-HeXAI modified perovskite films.

Samples	E_{onset} (eV)	E_{cutoff} (eV)	E_{VB} (eV)	E_{CB} (eV)	$E_{F\text{-edge}}$ (eV)
Control	0.73	16.93	-5.02	-3.47	-4.29
Hybrid anti-solvent	0.63	16.80	-5.05	-3.50	-4.42
Target	0.67	16.63	-5.26	-3.71	-4.59

Table S6. Calculated surface energies of (001), (011) and (012) crystal facets modified by n-HeXAI ligands

Crystal plane	Surface Energy (eV)	
(001)	-9.06E-01	exothermic
(011)	-4.09E-01	exothermic
(012)	-7.30E-01	exothermic

Note S1. FF loss analysis

According to the assumption of S-Q limit, the FF loss is mainly determined by the non-radiative loss and the charge transfer loss. The higher the value of the maximum FF (FF_{max}), the lower the non-radiative recombination loss of the PSCs. FF_{max} can be calculated by following equation:

$$FF_{max} = \frac{v_{oc} - ln(v_{oc} + 0.72)}{v_{oc} + 1} \tag{1}$$

$$v_{oc} = \frac{V_{oc}}{nK_BT/q} \tag{2}$$

Where K_B, T and q denotes Boltzmann constant, the absolute temperature (300 K) and elementary charge. n is the ideal factor that is fitted from the V_{OC} as a logarithmic function of light intensity, which is shown in **Figure 2c**.

Note S2. Nucleation

According to the classical crystal nucleation theory, the total free energy of nucleus formation (ΔG) consists of a volume term (ΔG_v, free energy difference between the nuclei and the solute in solution) and a surface term (ΔG_s, free energy difference between the nuclei surface and the bulk of the nuclei), as given in the following equation:

$$\Delta G = \Delta G_s + \Delta G_v = 4\pi r^2\sigma - \frac{4}{3}\pi r^3 K_B T\frac{\ln{(S)}}{V} \tag{3}$$

Where r, σ, K_B, T, S and V denote the radius of the nucleus, the surface energy, the Boltzmann constant, the absolute temperature, the supersaturation ratio and the molar volume of the nucleus, respectively. **Figure S22** exhibits a graph of ΔG as a function of r.

Reference

1. G. Kresse and J. Furthmüller, *Phy. Rev. B*, 1996, **54**, 11169-11186.
2. W. Kohn and L. J. Sham, *Phy. Rev.*, 1965, **140**, A1133-A1138.
3. P. Hohenberg and W. Kohn, *Phy. Rev.*, 1964, **136**, B864-B871.
4. J. P. Perdew, K. Burke and M. Ernzerhof, *Phys. Rev. Lett.*, 1996, **77**, 3865-3868.
5. V. Wang, N. Xu, J.-C. Liu, G. Tang and W.-T. Geng, *Comput. Phys. Commun.*, 2021, **267**, 108033.
6. J. Zhou, L. Tan, Y. Liu, H. Li, X. Liu, M. Li, S. Wang, Y. Zhang, C. Jiang, R. Hua, W. Tress, S. Meloni and C. Yi, *Joule*, 2024, **8**, 1691-1706.
7. M. J. Paik, Y. Y. Kim, J. Kim, J. Park and S. I. Seok, *Joule*, 2024, **8**, 2073-2086.
8. X. Li, S. Gao, X. Wu, Q. Liu, L. Zhu, C. Wang, Y. Wang, Z. Liu, W. Chen, X. Li, P. Xiao, Q. Huang, T. Chen, Z. Li, X. Gao, Z. Xiao, Y. Lu, X. Zeng, S. Xiao, Z. Zhu and S. Yang, *Joule*, 2024, **8**, 3169-3185.
9. Y. S. Shin, J. W. Song, D. G. Lee, J. Lee, J. Seo, J. Roe, G. Y. Shin, D. Kim, J. Yeop, D. Lee, M. Kim, Y. Jo, H. Jang, J. G. Son, W. Lee, J. Son, S. Park, S. Cho, T. J. Shin, G.-H. Kim, J. Y. Kim, T. K. Lee, M. Grätzel and D. S. Kim, *Joule*, 2025, **9**, 101779.
10. B. Li, Y. Yao, C. Kan, P. Hang, J. Xie, Q. Yin, D. Zhang, X. Yu and D. Yang, *Joule*, 2025, **9** 101780.
11. B. Wen, T. Chen, Q. Yin, J. Xie, C. Dai, R. Lin, S. Zhou, J. Yu and P. Gao, *Nat. Commun.*, 2024, **15**, 7720.
12. Z. Qu, Y. Zhao, F. Ma, L. Mei, X.-K. Chen, H. Zhou, X. Chu, Y. Yang, Q. Jiang,

X. Zhang and J. You, *Nat. Commun.*, 2024, **15**, 8620.

13. J. Li, C. Jin, R. Jiang, J. Su, T. Tian, C. Yin, J. Meng, Z. Kou, S. Bai, P. Müller-Buschbaum, F. Huang, L. Mai, Y.-B. Cheng and T. Bu, *Nat. Energy*, 2024, **9**, 1540-1550.
14. Y. Tian, X. Zhang, K. Zhao, X. Miao, T. Deng, W. Fan, D. Jin, X. Jiang, S. Zhong, X. Wang, S. Wang, P. Shi, L. Tian, L. Yao, S. Gong, X. Yu, X. Gao, Z. Chen, X. Chen, Y. Lu, V. Shrote, Y. Yang, D. Yang, R. Wang and J. Xue, *Nat. Photonics*, 2024, **18**, 960-966.
15. S. Li, Y. Jiang, J. Xu, D. Wang, Z. Ding, T. Zhu, B. Chen, Y. Yang, M. Wei, R. Guo, Y. Hou, Y. Chen, C. Sun, K. Wei, S. M. H. Qaid, H. Lu, H. Tan, D. Di, J. Chen, M. Grätzel, E. H. Sargent and M. Yuan, *Nature*, 2024, **635**, 82-88.
16. Q. Li, H. Liu, C.-H. Hou, H. Yan, S. Li, P. Chen, H. Xu, W.-Y. Yu, Y. Zhao, Y. Sui, Q. Zhong, Y. Ji, J.-J. Shyue, S. Jia, B. Yang, P. Tang, Q. Gong, L. Zhao and R. Zhu, *Nat. Energy*, 2024, **9**, 1506-1516.
17. C. Gong, H. Li, Z. Xu, Y. Li, H. Wang, Q. Zhuang, A. Wang, Z. Li, Z. Guo, C. Zhang, B. Wang, X. Li and Z. Zang, *Nat. Commun.*, 2024, **15**, 9154.
18. G. Qu, S. Cai, Y. Qiao, D. Wang, S. Gong, D. Khan, Y. Wang, K. Jiang, Q. Chen, L. Zhang, Y.-G. Wang, X. Chen, A. K. Y. Jen and Z.-X. Xu, *Joule*, 2024, **8**, 2123-2134.
19. M. Tao, Y. Wang, K. Zhang, Z. Song, Y. Lan, H. Guo, L. Guo, X. Zhang, J. Wei, D. Cao and Y. Song, *Joule*, 2024, **8**, 3142-3152.
20. B. Li, Q. Liu, J. Gong, S. Li, C. Zhang, D. Gao, Z. Chen, Z. Li, X. Wu, D. Zhao,

Z. Yu, X. Li, Y. Wang, H. Lu, X. C. Zeng and Z. Zhu, *Nat. Commun.*, 2024, **15**, 2753.

21. C. Gong, H. Li, H. Wang, C. Zhang, Q. Zhuang, A. Wang, Z. Xu, W. Cai, R. Li, X. Li and Z. Zang, *Nat. Commun.*, 2024, **15**, 4922.
22. S. Xiong, F. Tian, F. Wang, A. Cao, Z. Chen, S. Jiang, D. Li, B. Xu, H. Wu, Y. Zhang, H. Qiao, Z. Ma, J. Tang, H. Zhu, Y. Yao, X. Liu, L. Zhang, Z. Sun, M. Fahlman, J. Chu, F. Gao and Q. Bao, *Nat. Commun.*, 2024, **15**, 5607.
23. R. Azmi, D. S. Utomo, B. Vishal, S. Zhumagali, P. Dally, A. M. Risqi, A. Prasetio, E. Ugur, F. Cao, I. F. Imran, A. A. Said, A. R. Pininti, A. S. Subbiah, E. Aydin, C. Xiao, S. I. Seok and S. De Wolf, *Nature*, 2024, **628**, 93-98.
24. W.-T. Wang, P. Holzhey, N. Zhou, Q. Zhang, S. Zhou, E. A. Duijnstee, K. J. Rietwyk, J.-Y. Lin, Y. Mu, Y. Zhang, U. Bach, C.-G. Wu, H. L. Yip, H. J. Snaith and S.-P. Feng, *Nature*, 2024, **632**, 294-300.
25. K. Zhao, Q. Liu, L. Yao, C. Değer, J. Shen, X. Zhang, P. Shi, Y. Tian, Y. Luo, J. Xu, J. Zhou, D. Jin, S. Wang, W. Fan, S. Zhang, S. Chu, X. Wang, L. Tian, R. Liu, L. Zhang, I. Yavuz, H.-f. Wang, D. Yang, R. Wang and J. Xue, *Nature*, 2024, **632**, 301-306.
26. S. Liu, J. Li, W. Xiao, R. Chen, Z. Sun, Y. Zhang, X. Lei, S. Hu, M. Kober-Czerny, J. Wang, F. Ren, Q. Zhou, H. Raza, Y. Gao, Y. Ji, S. Li, H. Li, L. Qiu, W. Huang, Y. Zhao, B. Xu, Z. Liu, H. J. Snaith, N.-G. Park and W. Chen, *Nature*, 2024, **632**, 536-542.
27. S. Li, Y. Xiao, R. Su, W. Xu, D. Luo, P. Huang, L. Dai, P. Chen, P. Caprioglio,

K. A. Elmestekawy, M. Dubajic, C. Chosy, J. Hu, I. Habib, A. Dasgupta, D. Guo, Y. Boeije, S. J. Zelewski, Z. Lu, T. Huang, Q. Li, J. Wang, H. Yan, H.-H. Chen, C. Li, B. A. I. Lewis, D. Wang, J. Wu, L. Zhao, B. Han, J. Wang, L. M. Herz, J. R. Durrant, K. S. Novoselov, Z.-H. Lu, Q. Gong, S. D. Stranks, H. J. Snaith and R. Zhu, *Nature*, 2024, **635**, 874-881.

28. S. Zhang, F. Ye, X. Wang, R. Chen, H. Zhang, L. Zhan, X. Jiang, Y. Li, X. Ji, S. Liu, M. Yu, F. Yu, Y. Zhang, R. Wu, Z. Liu, Z. Ning, D. Neher, L. Han, Y. Lin, H. Tian, W. Chen, M. Stolterfoht, L. Zhang, W.-H. Zhu and Y. Wu, *Science*, 2023, **380**, 404-409.
29. S. M. Park, M. Wei, J. Xu, H. R. Atapattu, F. T. Eickemeyer, K. Darabi, L. Grater, Y. Yang, C. Liu, S. Teale, B. Chen, H. Chen, T. Wang, L. Zeng, A. Maxwell, Z. Wang, K. R. Rao, Z. Cai, S. M. Zakeeruddin, J. T. Pham, C. M. Risko, A. Amassian, M. G. Kanatzidis, K. R. Graham, M. Grätzel and E. H. Sargent, *Science*, 2023, **381**, 209-215.
30. P. Zhu, D. Wang, Y. Zhang, Z. Liang, J. Li, J. Zeng, J. Zhang, Y. Xu, S. Wu, Z. Liu, X. Zhou, B. Hu, F. He, L. Zhang, X. Pan, X. Wang, N.-G. Park and B. Xu, *Science*, 2024, **383**, 524-531.
31. S. Yu, Z. Xiong, H. Zhou, Q. Zhang, Z. Wang, F. Ma, Z. Qu, Y. Zhao, X. Chu, X. Zhang and J. You, *Science*, 2023, **382**, 1399-1404.
32. H. Tang, Z. Shen, Y. Shen, G. Yan, Y. Wang, Q. Han and L. Han, *Science*, 2024, **383**, 1236-1240.
33. C. Liu, Y. Yang, H. Chen, J. Xu, A. Liu, A. S. R. Bati, H. Zhu, L. Grater, S. S.

Hadke, C. Huang, V. K. Sangwan, T. Cai, D. Shin, L. X. Chen, M. C. Hersam, C. A. Mirkin, B. Chen, M. G. Kanatzidis and E. H. Sargent, *Science*, 2023, **382**, 810-815.

34. H. Chen, C. Liu, J. Xu, A. Maxwell, W. Zhou, Y. Yang, Q. Zhou, A. S. R. Bati, H. Wan, Z. Wang, L. Zeng, J. Wang, P. Serles, Y. Liu, S. Teale, Y. Liu, M. I. Saidaminov, M. Li, N. Rolston, S. Hoogland, T. Filleter, M. G. Kanatzidis, B. Chen, Z. Ning and E. H. Sargent, *Science*, 2024, **384**, 189-193.
35. Z. Li, X. Sun, X. Zheng, B. Li, D. Gao, S. Zhang, X. Wu, S. Li, J. Gong, J. M. Luther, Z. a. Li and Z. Zhu, *Science*, 2023, **382**, 284-289.
36. C. Liu, Y. Yang, H. Chen, I. Spanopoulos, A. S. R. Bati, I. W. Gilley, J. Chen, A. Maxwell, B. Vishal, R. P. Reynolds, T. E. Wiggins, Z. Wang, C. Huang, J. Fletcher, Y. Liu, L. X. Chen, S. De Wolf, B. Chen, D. Zheng, T. J. Marks, A. Facchetti, E. H. Sargent and M. G. Kanatzidis, *Nature*, 2024, **633**, 359-364.
37. S. Cai, Z. Li, Y. Zhang, T. Liu, P. Wang, M.-G. Ju, S. Pang, S. P. Lau, X. C. Zeng and Y. Zhou, *Nat. Commun.*, 2024, **15**, 2329.
38. L. Ye, J. Wu, S. Catalán-Gómez, L. Yuan, R. Sun, R. Chen, Z. Liu, J. M. Ulloa, A. Hierro, P. Guo, Y. Zhou and H. Wang, *Nat. Commun.*, 2024, **15**, 7889.
39. J. Zhou, L. Tan, Y. Liu, H. Li, X. Liu, M. Li, S. Wang, Y. Zhang, C. Jiang, R. Hua, W. Tress, S. Meloni and C. Yi, *Joule*, 2024, **8**, 1691-1706.
40. X. Chen, F. Yang, L. Yuan, S. Huang, H. Gu, X. Wu, Y. Shen, Y. Chen, N. Li, H.-J. Egelhaaf, C. J. Brabec, R. Zhang, F. Gao, Y. Li and Y. Li, *Joule*, 2024, **8**, 2265-2282.

41. Q. Xiong, X. Huang, C. Wang, Q. Zhou, Y. Gang, T. Li, C. Hu, N. Zhang, X. Wang, J. Wu, Z. Su, X. Gao, X. Li, N. Zheng and P. Gao, *Joule*, 2024, **8**, 817-834.
42. H. Song, H.-B. Kim, S. C. Cho, J. Lee, J. Yang, W. H. Jeong, J. Y. Won, H. I. Jeong, J. Yeop, J. Y. Kim, B. J. Lawrie, M. Ahmadi, B. R. Lee, M. Kim, S. J. Choi, D. S. Kim, M. Lee, S. U. Lee, Y. Jo and H. Choi, *Joule*, 2024, **8**, 2283-2303.
43. J. Fang, D. Lin, G. Xie, S. Li, H. Li, X. Wang, D. Wang, N. Huang, H. Peng, L. Gan, Y. Zhu, S. He and L. Qiu, *Energy Environ. Sci.*, 2024, **17**, 7829-7837.
44. J. Li, B. Fan, X. Liu, Y. Liu, Z. Xing, C. Gong, Z. Chu, L. Li, X. Meng, R. Guo, F. Wang, X. Hu and Y. Chen, *Energy Environ. Sci.*, 2024, **17**, 6821-6832.
45. Z. Wan, B. Ding, J. Su, Z. Su, Z. Li, C. Jia, Z. Jiang, Q. Qin, M. Zhang, J. Shi, H. Wu, C. Zhi, F. Wang, C. Li, L. Du, C. Zhang, Y. Ding, C. Li, X. Gao, C. Xiao, J. Chang, M. K. Nazeeruddin and Z. Li, *Energy Environ. Sci.*, 2024, **17**, 6302-6313.
46. Y. Ding, E. Feng, S. Lu, J. Chang, C. Long, S. Tong, H. Li and J. Yang, *Energy Environ. Sci.*, 2024, **17**, 9268-9277.